

# EMULATING NUCLEAR EMISSION WITH A PULSED LASER

by

Benjamin J. Hockman

A thesis submitted to the Faculty of the University of Delaware in partial fulfillment of the requirements for the degree of Honors Bachelor of Mechanical Engineering with Distinction

Spring 2013

© 2013 Benjamin J. Hockman  
All Rights Reserved

**EMULATING NUCLEAR EMISSION WITH A PULSED LASER**

by

Benjamin J. Hockman

Approved: \_\_\_\_\_  
Herbert G. Tanner, Ph.D.  
Professor in charge of thesis on behalf of the Advisory Committee

Approved: \_\_\_\_\_  
Ioannis Poulakakis , Ph.D.  
Committee member from the Department of Mechanical Engineering

Approved: \_\_\_\_\_  
Victor N. Kaliakin, Ph.D.  
Committee member from the Board of Senior Thesis Readers

Approved: \_\_\_\_\_  
Michael Arnold, Ph.D.  
Director, University Honors Program

## ACKNOWLEDGMENTS

First, I would like to thank my advisor, Dr. Tanner for giving me this great opportunity to perform research in his lab and for his continued guidance and support. I would also like to thank my second and third readers, Dr. Poulakakis and Dr. Kaliakin for their support and assistance in completing this thesis.

I would also like to thank Jianxin Sun for his tremendous help in the lab running experiments, and all of the other students in the lab for putting up with the distracting laser flashes.

Finally I would like to thank master machinist, Steve Beard, for his patience with me in the shop, and the Undergraduate Research Program for giving me the opportunity to engage in two years of interesting research.

## TABLE OF CONTENTS

<b>LIST OF FIGURES</b> . . . . .	<b>vi</b>
<b>ABSTRACT</b> . . . . .	<b>viii</b>
<b>Chapter</b>	
<b>1 INTRODUCTION</b> . . . . .	<b>1</b>
1.1 Motivation . . . . .	1
1.2 Detecting Poisson Emissions . . . . .	2
1.2.1 The Underlying Physics . . . . .	2
1.2.2 The Poisson Process . . . . .	4
1.2.3 Detection . . . . .	6
1.2.4 Hypothesis Testing . . . . .	8
1.3 Related Work . . . . .	11
1.4 Scope and Organization . . . . .	14
<b>2 PROBLEM STATEMENT</b> . . . . .	<b>16</b>
<b>3 TECHNICAL APPROACH</b> . . . . .	<b>19</b>
3.1 Device Design . . . . .	19
3.2 Directional Randomness . . . . .	21
3.3 Mixing Background and Source Signals . . . . .	22
3.4 Distance from Sensor to Source . . . . .	23
3.5 Scaling . . . . .	24
3.6 Computational Delays and Frequency Limitations . . . . .	26
<b>4 EXPERIMENTAL RESULTS</b> . . . . .	<b>27</b>
4.1 Conforming to Poisson Statistics . . . . .	27
4.2 Application to Static Detection . . . . .	31
4.3 Detection of a Mobile Source . . . . .	35

<b>5 CONCLUSION . . . . .</b>	<b>40</b>
<b>REFERENCES . . . . .</b>	<b>42</b>
<b>Appendix</b>	
<b>MATLAB™ CONTROL PSEUDOCODE . . . . .</b>	<b>44</b>

## LIST OF FIGURES

1.1	A schematic diagram of a Geiger counter . . . . .	4
1.2	Sample Poisson counting process with mean $\lambda = 4Hz$ ; the vertical axis is the cumulative number of counts and the horizontal axis is time. . . . .	5
1.3	Sample Poisson distribution with means $\lambda = 1, 4, 10$ cpm; the vertical axis is the probability of $k$ occurrences within 1 minute; Note: the function is only defined at integer values of $k$ . The connecting lines are only guides for the eye. . . . .	5
1.4	A MATLAB <sup>TM</sup> simulation of a Poisson process with $\lambda_1 = 300$ Hz at $t > 0$ and $\lambda_2 = 600$ Hz at $t > 1$ . . . . .	7
1.5	Example of two Poisson processes simulations with the same background levels ( $\lambda_1$ ) but different source signal strength ( $\lambda_2$ ). The top plots show the counting step plot with the vertical lines marking the region when the source ( $\lambda_2$ ) is present. The lower plots show the time-varying log-likelihood ratio in blue and the threshold corresponding to 99% confidence in red. . . . .	12
3.1	Solidworks <sup>TM</sup> rendering of the experimental setup: $r$ is the distance between sensor and mirror; $w$ is the sensitive width of sensor. . . . .	20
3.2	(a) Schematic of laser emission in $\mathbb{R}^2$ ; (b) element of laser beam scattering . . . . .	23
4.1	(a) bead of Vaseline glass; (b) Geiger counter . . . . .	28
4.2	A 24-hour sample of background radiation ( $n \approx 18,000$ ) as measured by a Geiger counter . . . . .	29
4.3	A three-hour sample from the laser device emitting Poisson background ( $n \approx 6,000$ ) . . . . .	29

4.4	Geiger counter samples in range of radioactive glass bead . . . . .	30
4.5	Mean intensity at sensor ( $\lambda + \beta$ ) vs. source distance . . . . .	31
4.6	Probability of detection vs. likelihood ratio threshold (log10 scale) in bead experiment at distances 1, 1.5, 2, 2.5, and 3 cm . . . . .	34
4.7	Probability of detection vs. likelihood ratio threshold (log10 scale) from experiments with the laser device at distances 4, 9, 16, 25, and 36 inches . . . . .	35
4.8	(a) laser device mounted on the iCreate <sup>TM</sup> ; (b) light sensor mounted on the Corobot <sup>TM</sup> . . . . .	36
4.9	Schematic of experiment with 1D source movement . . . . .	37
4.10	Picture of a mobile detection experiment with one mobile sensor and four stationary sensors . . . . .	37
4.11	Log likelihood ratios based on data collected from 4 sensor groupings: two from just the four static sensors (one just background and one including the source), and two from all 5 sensors (one just background and one including the source) . . . . .	38

## ABSTRACT

The problem of detecting hazardous radioactive materials is receiving considerable attention due to emerging threats of clandestine nuclear attacks. Protection against these threats requires a multilayered defense approach, combining border security through cargo screening with overseas nonproliferation enforcement. Current technology is insufficient for applications that involve searching or mapping in unstructured environments. Instead of using large expensive radiographic imaging sensors at controlled security stations, many applications require the use of multiple less sophisticated sensors. These sensor networks can be mobile in general and can adaptively reconfigure themselves to collect more useful measurements (e.g. moving sensors closer to inspect a potential source).

Determining how to optimally control sensor networks and process collected information for quick and confident detection is a difficult problem that has driven recent theoretical developments. And although the physics behind emission and sensing radiation is well understood and our models typically work well, there is still a need for experimental testing of newly developed theory. Not only can experimentation validate our expectations of system behavior, but it can also provide valuable insight for improving our models and control strategies. However, using actual fissile materials for experiments would be hazardous and impractical.

The aim of this research is to develop a novel system that emulates the process of nuclear emission to use as an innocuous proxy for experimental testing. The device developed uses a modulated laser pointer to produce sporadic pulses of light and a rotating mirror that reflects each pulse in a random direction, mimicking the way in which gamma rays are emitted from a radiation source. The performance of this emulation is compared to that of a weakly radioactive source through side by side

experiments. First, the pulse frequency distribution is shown to conform to the desired Poisson process, which is the underlying process used to model weak radiation detection. Next, the distance-dissipation effect is verified through static tests at various distances. The device is then applied to two simple detection regimes: static fixed interval detection and detection of a source moving in a straight line with a combination of static and mobile sensors. The results show a strong agreement with simulations and thus, the device is concluded to be a viable proxy for experimentation. The pros and cons of using the device are discussed and careful attention is given to analyzing the conditions under which it can be used.

# Chapter 1

## INTRODUCTION

### 1.1 Motivation

The post 9/11 threat of nuclear terrorism is being taken very seriously by the U.S. government. In 2005, the Domestic Nuclear Detection Office was established and over \$3 billion has been invested in R&D for improved nuclear threat detection systems [1]. While preventing nuclear attacks requires a multilayered approach which combines policy, intelligence, and enforcement, a principle component of defense is our capability of detecting these potentially hazardous materials. Just like any other type of illicit cargo such as guns or drugs, terrorists would presumably conceal radiological materials when crossing border security checkpoints. However, unlike guns and drugs, radiological materials are characterized by their continuous decay and electromagnetic emissions, which can be detected at a distance with the right type of sensors. But because these emissions can be shielded with heavy metals and decay over distances, their “detectability” depends on what types of sensors we use and how we use them.

Generally speaking, this problem can be approached from two angles. The first and most obvious approach is to improve the capabilities of individual sensors, which includes technology such as radiation-based spectroscopy, radiographic imaging, active interrogation etc. The goal on this front is to identify, isolate, and amplify signals coming from a potential source to differentiate them from background noise. Research in sensor technology has been carried out for over 60 years, and recent advances in many areas hold promise for significant improvements in sensor capabilities. However, the inescapable trend in this research is that, in order to improve sensor performance, they must be larger, heavier, and more expensive. As a result, advanced technology is

limited to stationary *Radiation Portal Monitors* (RPMs), which are typically located at cargo screening checkpoints along international borders. RPMs have a high rate of false alarms and are very slow, requiring vehicles to slow down or stop temporarily.

The second approach is to employ networks of smaller sensors, which can be cooperatively coordinated to collect more information about the environment. One advantage of such an approach is that sensor networks can be spatially distributed and cover a larger region than stationary point sensors. And because individual sensors are smaller, they can be mobile and adaptively move towards regions of greater interest. This opens up a whole realm of possibilities for radiation detection, allowing for new applications in unstructured and dynamically changing environments. For example, a network of sensor-equipped mobile robots could be deployed in a suspicious environment to search for threats before humans move in. However, it also forces us to ask some new and difficult questions such as how to control such multi-agent systems, how to optimally fuse their measurements to make a collaborative decision, and how to use collected information to plan trajectories. These questions have only recently been investigated and there are still many open problems to be addressed.

## **1.2 Detecting Poisson Emissions**

### **1.2.1 The Underlying Physics**

As radioactive materials decay, they emit alpha particles, beta particles, and gamma rays. Sensors exist to detect all three forms of emissions, but alpha and beta particles are easily shielded. It typically takes thick layers of heavy metals such as lead to shield high energy gamma rays. So for detecting these materials at large distances, gamma ray sensors are preferred. Also, as with any type of electromagnetic emissions, the intensity of the source dissipates as the observed distance increases, which scales with the inverse square of the distance. So proximity is highly advantageous from a detection standpoint.

So why are weak signals problematic? It isn't a matter of exceeding a sensitivity threshold, as is often the case with light sensors. It is because they blend in easily with

naturally occurring background radiation. Environmental radiation is usually weak enough that it isn't harmful to humans, and it can come from sources like cosmic radiation, minerals in the bedrock, or even building materials. Background levels vary from location to location and can even fluctuate throughout the day. From a detection standpoint, the background radiation is simply everything that is not the source in question. However, because sensors cannot usually discern the origin of incident gamma rays, the signals they measure are simply the additive intensities of both source and background signals. The *signal to noise ratio* (SNR) is a common metric for describing the relative intensities of the two signals. High SNRs indicate a strong source signal and low SNRs indicate a weaker signal, and it has a strong correlation with the “detectability” of a source.

The most common types of sensors used for detecting gamma radiation are called *Geiger counters*. Invented over 80 years ago, Geiger counters are simple sensors that consist of a tube filled with inert gas that briefly conducts electricity when a high-energy ionized particle strikes it (see Fig. 1.1). A cathode and anode are separated by this inert gas so that each gamma ray captured produces a pulse of electricity. The discrete pulses give rise to a counting process, which is fundamentally different from the way that sensors typically work at other wavelengths. Photoresistors, for example, are the most common type of sensor for visible light and they are made of a photosensitive material that changes resistivity in proportion to the mean light intensity, or photon flux. This technique of flux measurement works well for most wavelengths because the intensities are typically large enough that photon “streams” can be well approximated by an average count rate. However, if the lights are dimmed low enough, the average photon flux becomes difficult to estimate because the separation between photons is large. This is the region that is most prevalent when dealing with low level gamma radiation. As an analogy, think of visible light as a steady flow of water through a hose and gamma radiation as a slowly dripping faucet. We would need different measurement techniques to estimate the flow rate of each. To put this difference in perspective, the units typically used for photon frequency in the gamma region is *counts*

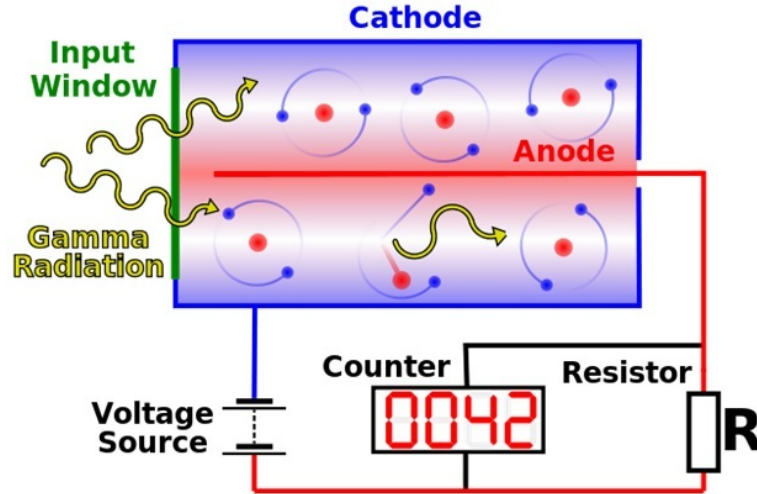


Figure 1.1: A schematic diagram of a Geiger counter

per minute (cpm), whereas visible light is often measured in  $GHz$  (billions of photons per second).

### 1.2.2 The Poisson Process

Since the direction that gamma rays are emitted from a source is random, it follows that the gamma rays received by a sensor are also random. And because the signal intensity can be defined as a mean frequency and collisions of gamma rays are independent, this phenomenon can be modeled as a *Poisson process*. A Poisson process is a stochastic process defined by the exponential probability density function (*PDF*) for the time between events with mean  $1/\lambda$  given by

$$P(x; \lambda) = \lambda e^{-\lambda x}, \quad x \geq 0 . \quad (1.1)$$

Figure 1.2 shows what the sensor would observe over time and Fig. 1.3 shows the resulting Poisson distribution for a few example means. In the context of radiation detection, the Poisson distribution governs the probability that a certain number of gamma rays will be measured over a given timespan.

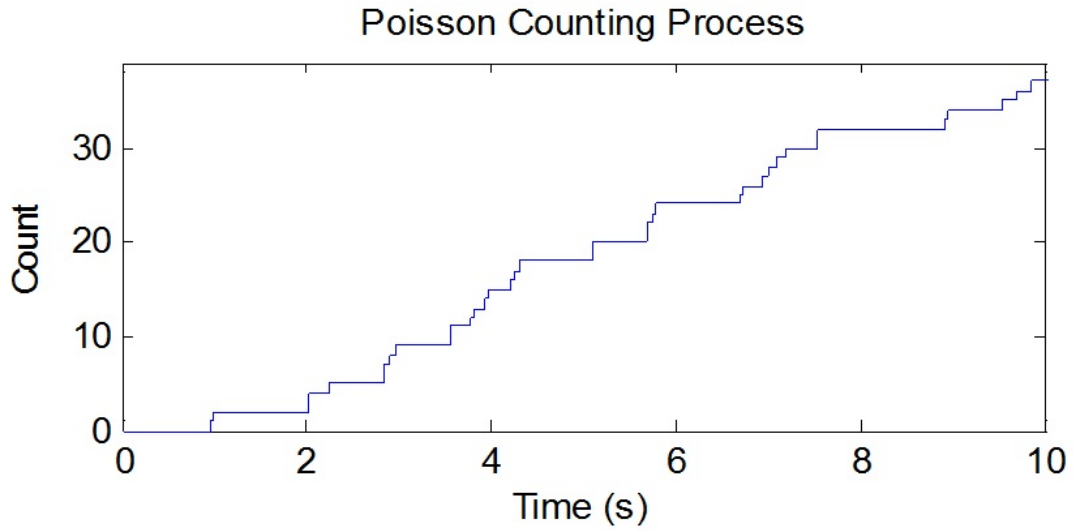


**Figure 1.2:** Sample Poisson counting process with mean  $\lambda = 4Hz$ ; the vertical axis is the cumulative number of counts and the horizontal axis is time.

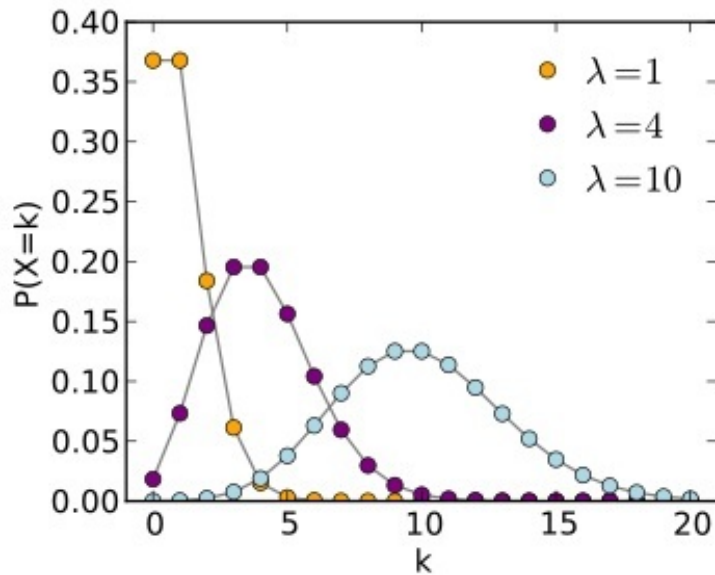


**Figure 1.3:** Sample Poisson distribution with means  $\lambda = 1, 4, 10$  cpm; the vertical axis is the probability of  $k$  occurrences within 1 minute; Note: the function is only defined at integer values of  $k$ . The connecting lines are only guides for the eye.

It turns out that Poisson processes are ubiquitous in modeling natural phenomena and are not restricted to describing radioactive decay. Generally, most continuous-time counting processes with independently occurring events can be well modeled with this process; some examples include the number of goals scored during a basketball game, hits on a web page, and the number of raindrops falling within a specified area [2].

### 1.2.3 Detection

In detection problems, it is usually the case that we need to simply determine whether or not there is an emitting source present. In other words, based on the information gathered by the sensors, is there more evidence to suggest that a source is present or not. Consider the following regime: we have two radiation sources generating independent Poisson emissions in parallel with intensities  $\lambda_1$  and  $\lambda_2$ . At  $t_0$ ,  $\lambda_1$  is turned on and at  $t_1 = 1$  s,  $\lambda_2$  is turned on. They both emit the same frequency gamma rays, such that a nearby sensor can only pick the sum of both emissions  $\lambda_1 + \lambda_2$ . Now suppose that this nearby sensor—with no knowledge of the binary states of each source—needs to decide between two hypotheses  $H_0$  and  $H_1$  at a given time  $T$  after the second source is turned on, where

(i)  $H_0$ : only  $\lambda_1$  is turned on, and

(ii)  $H_1$ : both  $\lambda_1$  and  $\lambda_2$  are turned on.

This is an instance of an inverse problem, posed as a binary hypothesis decision problem.

An example of what this sensor might observe in this *fixed interval detection paradigm* is illustrated in Fig. 1.4 for three values of  $T$ . These three plots help to visualize why the ability of a sensor to make a decision between  $H_0$  and  $H_1$  is highly dependent on the observation interval  $T$ . The naked eye can tell that there is clearly a change in count rate for  $T = 1$ , but it becomes less obvious at  $T = 0.1$  and almost indistinguishable at  $T = 0.01$ . Similarly, any decision made between  $H_0$  and  $H_1$  exhibits

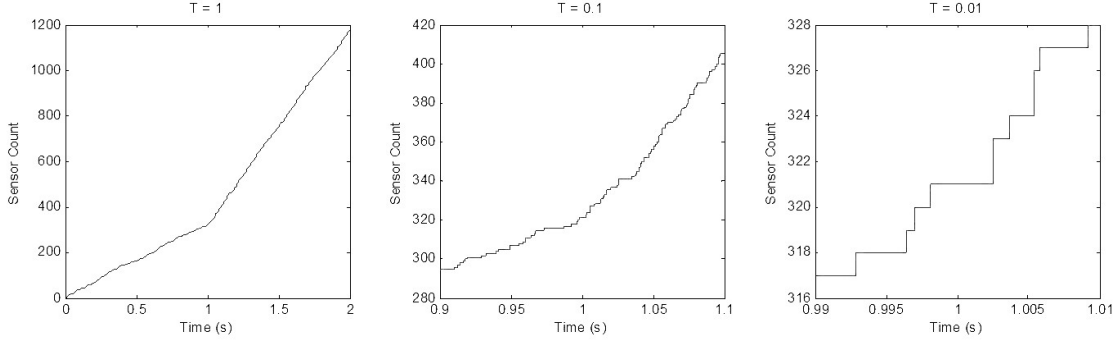


**Figure 1.4:** A MATLAB<sup>TM</sup> simulation of a Poisson process with  $\lambda_1 = 300$  Hz at  $t > 0$  and  $\lambda_2 = 600$  Hz at  $t > 1$ .

a confidence level roughly proportional to  $T$ . Indeed, the fundamental goal of the binary detection problem is to make a decision between the two hypotheses as quick as possible while minimizing the chances of error.

This emission regime has many practical applications when dealing with the detection of a radiation source. Physically, we can think of  $\lambda_1$  as the background radiation that is confounding the source ( $\lambda_2$ ) we are trying to detect. We will denote these two emissions with the letters  $\beta$  and  $R$ , respectively. In general, the background intensity  $\beta$  is non-homogeneous and position dependent (i.e.  $\beta = \beta(\vec{X}, t)$ ,  $\vec{X} \in \mathbb{R}^3$ ), but for most cases we can assume  $\beta$  to vary only with position, where the radiation map  $\beta(\vec{X})$  is known [3].

The radiation due to the source is also non-homogeneous in nature and is presumed to be proportional to the square of the distance of the sensor from the source (i.e.  $R \propto 1/r^2$ )<sup>1</sup> [4]. This reflects the dispersion of gamma ray density from a point source in  $\mathbb{R}^3$ . Therefore, it is important to distinguish between the “source intensity” and the “perceived intensity.” The source intensity is a physical property of the source material, whereas the perceived intensity is a function of the source intensity and several other factors such as the distance, degree of shielding, and size of the sensor. So

---

<sup>1</sup> Relationship suggests that  $R$  increases unboundedly as  $r \rightarrow 0$ , but is valid under the assumption that the sensor maintains a minimum distance  $\delta > 0$  from the source. A better relationship is given in chap. 2

even though a weak source signal is observed, it may still be a very strong source that is either shielded or sufficiently far from the sensor. In fact, many important applications of low-level detection such as mobile searches for dirty bombs or passive surveillance screening for hazardous radioactive materials [5] deal with high intensity sources observed at a distance over a short period of time, making them more difficult to detect. The  $1/r^2$  relationship suggests that there are two ways to enhance the intensity of the source signal: (1) make better sensors or (2) move the sensors closer to the source. This project focuses on the later.

#### 1.2.4 Hypothesis Testing

We have already seen that signals generated by radiation sensors produce a discrete counting process and that estimating the mean count frequency of the signal takes time. Consequently, to test the two hypothesis,

$$(i) H_0: \lambda = \lambda_0$$

$$(ii) H_1: \lambda = \lambda_1$$

we cannot simply query the sensors at a point in time. Rather, a sequential testing method is typically used in which the data is evaluated as it is collected, and a conclusion is reached when the data provides enough evidence to support either (i) or (ii) with a certain level of confidence. When the PDFs for both  $\lambda_0$  and  $\lambda_1$  are known explicitly, the procedure is known as the *sequential probability ratio test* (SPRT) [6]. Developed by Wald in the early 1950s, the SPRT method takes consecutive data samples and calculates the probability that the sample ( $x_i$ ) belongs to each of the PDFs ( $f_{\lambda_0}(x)$  and  $f_{\lambda_1}(x)$ ). A statistic called the log-likelihood ratio ( $\log \Lambda_i$ ) is then computed and the cumulative sum of log-likelihood ratios gives us the log-likelihood function (LLF),

$$S_i = S_{i-1} + \log \Lambda_i \tag{1.2}$$

The LLF constantly changes as the sensors pick up new information—increasing when there is more evidence to support  $H_1$  and decreasing when there is more evidence to support  $H_0$ . When  $S_i$  eventually exceeds either the upper ( $b$ ) or lower ( $a$ ) threshold, a choice between  $H_0$  and  $H_1$  is finally made. Therefore, the stopping rule says

$$\begin{aligned} a < S_i < b & : \text{ continue monitoring} \\ S_i \geq b & : \text{ accept } H_1 \\ S_i \leq a & : \text{ accept } H_0 \end{aligned}$$

where  $a$  and  $b$  ( $0 < a < b < \infty$ ) are dependent on the desired probabilities of type I ( $P_{FA}$ ) and type II ( $P_{FN}$ ) errors. In radiation detection, these errors correspond to the rates of false alarms and false negatives, and  $P_{FA}$  and  $P_{FN}$  are chosen to control the probability of these errors. There is therefore a tradeoff between detection speed and error minimization because it takes longer for the LLF to reach extreme values. Thresholds  $a$  and  $b$  are calculated as<sup>2</sup>

$$a \approx \log \frac{P_{FN}}{1 - P_{FA}} \quad \text{and} \quad b \approx \log \frac{1 - P_{FN}}{P_{FA}} \quad . \quad (1.3)$$

Let us consider a simple example of how this would be applied to the case of radiation detection. For this example, we will take the background intensity ( $\lambda_0$ ) and source signal intensity ( $\lambda_1 - \lambda_0$ ) to be known *a priori* (which is not true in general). The sequential sampling technique could either be the number of gamma rays observed within a given time frame or simply the time between each consecutive gamma ray arrival. Considering a sample ( $x_i$ ) to be the time between consecutive counts, we must use the exponential distribution for  $P(x; \lambda_0)$  and  $P(x; \lambda_1)$  as given by (1.1). For one

---

<sup>2</sup> Approximation is used for the discrete case when the LLF may cross the threshold between samples. Equality holds for the continuous case.

sample, the log-likelihood ratio is

$$\begin{aligned}
\log \Lambda(x_i) &= \log \left[ \frac{P(x_i; \lambda_1)}{P(x_i; \lambda_0)} \right] \\
&= \log \left[ \frac{\lambda_1 \exp(-\lambda_1 x_i)}{\lambda_0 \exp(-\lambda_0 x_i)} \right] \\
&= \log \left[ \frac{\lambda_1}{\lambda_0} \exp(\lambda_0 x_i - \lambda_1 x_i) \right] \\
&= (\lambda_0 - \lambda_1)x_i + \log \frac{\lambda_1}{\lambda_0}
\end{aligned} \tag{1.4}$$

and the LLF is

$$\begin{aligned}
S_n &= \sum_{i=1}^n \log \Lambda(x_i) \\
&= (\lambda_0 - \lambda_1) \sum_{i=1}^n x_i + n \log \frac{\lambda_1}{\lambda_0} .
\end{aligned} \tag{1.5}$$

So according to the stopping rule,

$$\begin{aligned}
a &< (\lambda_0 - \lambda_1) \sum_{i=1}^n x_i + n \log \frac{\lambda_1}{\lambda_0} < b \\
\log \frac{1-P_{FN}}{P_{FA}} - n \log \frac{\lambda_1}{\lambda_0} &< (\lambda_0 - \lambda_1) \sum_{i=1}^n x_i < \log \frac{P_{FN}}{1-P_{FA}} - n \log \frac{\lambda_1}{\lambda_0} .
\end{aligned} \tag{1.6}$$

This traditional SPRT approach works well for cases where both background and source intensity can be well approximated. But in most cases of radiation detection, the source intensity is not known *a priori*. Typically, an object can be identified as a potential source and investigated to determine if local sensors produce *higher than normal* count rates. For this case, a more appropriate hypothesis to test is,

$$(i) \ H_0: \lambda = \beta$$

$$(ii) \ H_1: \lambda > \beta$$

This is a one sided hypothesis test because there is no physical significance to observing a signal weaker than the background. One application that could use this

hypothesis test is a simple passive radiation sensor with no knowledge of the potential existence or location of a source. It would simply send out an alert when local radiation levels are high enough to reject  $H_0$ . The approach to computing the log-likelihood ratio for this case is similar to the previous example, and can be found in [7].

To illustrate the impact that source signal strength has on detection, consider the four graphs in Fig. 1.5. The two plots on the left show the results of a Poisson process simulation with  $\text{SNR} = 1$ , and the two on the right show the results for  $\text{SNR} = 1/2$ . The log-likelihood ratio in the  $\text{SNR} = 1$  simulation crossed the threshold to reject  $H_0$ , but it did not in the  $\text{SNR} = 1/2$  simulation. In other words, the stronger signal is detected and the weaker signal is not, as we would expect. The selection of the threshold depends entirely on the situation and the relative penalties for false alarms and missed detections. A lower threshold will decrease the probability of missed detections, but it also increases the probability of false alarms. In practice, higher thresholds are set to minimize the probability of false alarms, directing the operators' attention to only serious threats.

Sequential testing works well in applications with passive monitoring, but it is not usually the best choice for situations where the potential sources are moving. In these cases, the SPRT may not have enough time to make a decision with a preset threshold and must make the best decision it can within a finite time interval of exposure. This is called the "fixed interval" hypothesis test, and it has the advantage of only considering data of interest, allowing maximum information to guide the hypothesis decision. This approach will be revisited in more detail in section 4.2.

### 1.3 Related Work

The mathematics of decision theory has grown significantly over the past few decades. Some of the groundwork done in Poisson detection can be attributed to its application in optical communications. It turns out that an avalanche photodiode (APD) attempting to pick up a modulated optical signal transmitted through a noisy medium often faces the same type of detection regime as a radiation sensor attempting

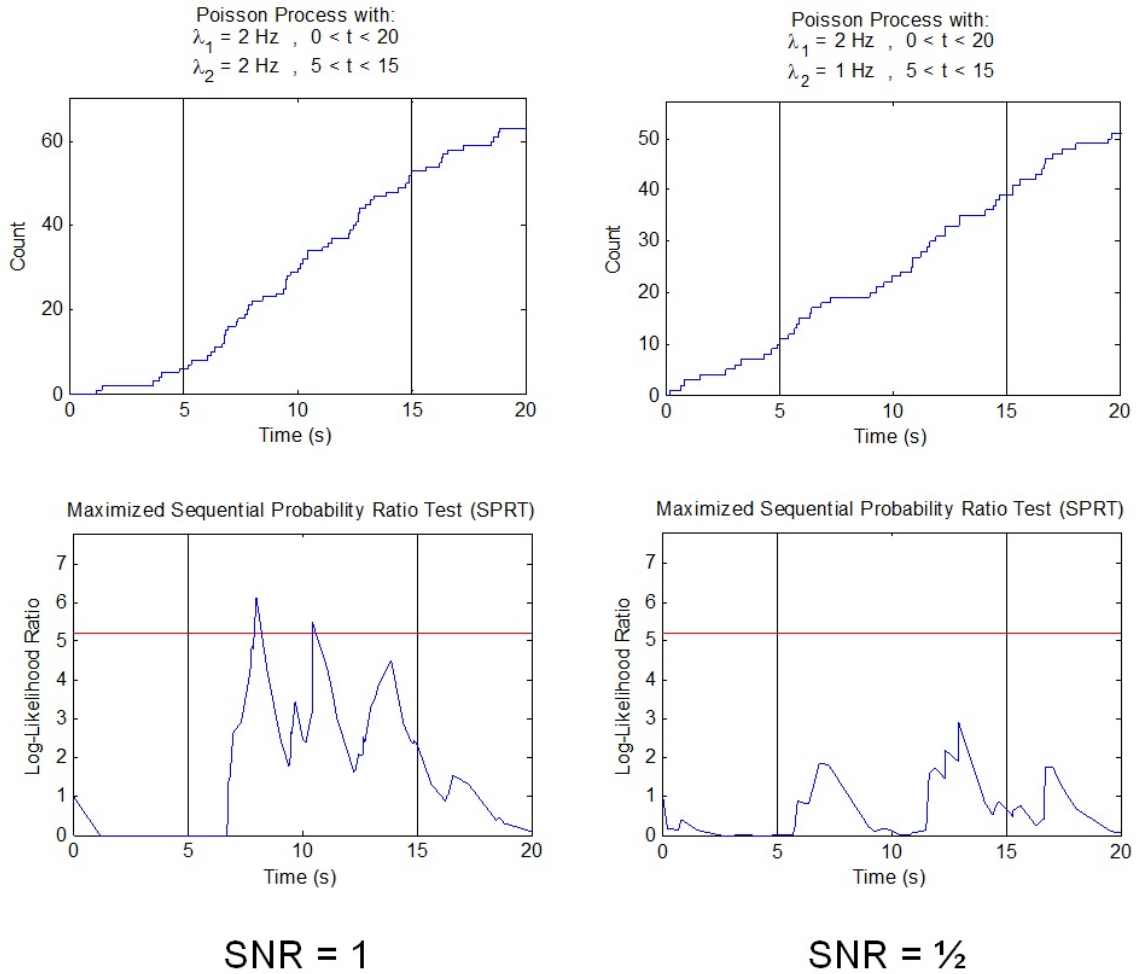


**Figure 1.5:** Example of two Poisson processes simulations with the same background levels ( $\lambda_1$ ) but different source signal strength ( $\lambda_2$ ). The top plots show the counting step plot with the vertical lines marking the region when the source ( $\lambda_2$ ) is present. The lower plots show the time-varying log-likelihood ratio in blue and the threshold corresponding to 99% confidence in red.

to pick out a weak signal from background noise [8, 9, 10, 11, 12]. The roots of sequential hypothesis testing were established in the early 1950s with Wald’s SPRT [6]. The test provides a time-optimal strategy for hypothesis testing of continuous processes such as the Poisson process. However, applying this method to different applications often requires more specific formulations, with adapted time-optimal solutions. For example, the regime outlined in Section 1.2.3 for a decision between two intensity values ( $\lambda_1$  or  $\lambda_1 + \lambda_2$ ) is known as the classical Bayesian approach and a formal solution to this problem can be found in [13].

Another popular testing method for this binary decision problem is the Neyman-Pearson test [14], which is discussed in the context of *fixed interval detection* in Section 1.2.4. A formal solution to this formulation can be adapted from a Bayesian approach and can be found in [7] (see also [15, 4] for network variants). Moreover, there can be various ways to define the detection specifications within each hypothesis formulation. For the case of radiation detection, we can think of a case where a sensor is given a finite time interval in which it must make a decision (fixed-interval test [16, 17]), or another case in which the sensor will only make a decision if its confidence level exceeds a threshold [18]. Other variables that also increase the complexity of the problem are:

- The sensor’s knowledge of a potential source
- The sensor’s knowledge of the source location and trajectory
- The directionality of a sensor (i.e. is it facing a certain direction)
- The orientation of multiple sensors in an array
- The ability of sensors to move in their environment
- The types of communication between sensors (i.e. networked or global)

These are just a few examples to illustrate the breadth of possibilities when implementing an optimal decision strategy. In fact, most of the work since the 1980s has

been more application focused to develop formal solutions for more specific formulations. Even within our narrow scope of radiation detection are numerous applications and parameters that can change the problem significantly.

However, there are still unanswered questions in the world of radiation detection. Consider the general example of detecting a mobile source that traverses a restricted area of observation in 2D. We know how to interpret the data gathered from a single sensor and even how to fuse data from multiple sensors, but the problem of detection with mobile sensor networks observing mobile targets is still open. Introducing mobility on the sensor side of sensor networks may significantly enhance their detection capabilities. It also raises many new questions such as how to optimally configure sensor positions and plan trajectories to gather a maximum amount of information or how to fuse data from a network of stationary and mobile sensors.

#### **1.4 Scope and Organization**

Since research in radiation detection is highly theoretical and the application of interest involves materials that cannot be readily handled, there is a gap between the theory that is developed in the academic world and practical implementation. There is a need for a bridge between theory and implementation—a method of experimentation that is safe to use in a laboratory setting. Not only can experimentation validate our expectations of detection performance, but it can also provide valuable insight for improving our models and control strategies.

There are weakly radioactive materials that are innocuous for humans and could be used for small scale experiments. Highly enriched uranium is the primary target for detection in the field, but many common items in our everyday lives are also weakly radioactive such as bananas, Brazil nuts, and cat litter. In the lab, we have a weakly radioactive bead of Vaseline glass about 1cm in diameter which can be picked up by a Geiger counter at a very close distance. However, the signal to noise ratio becomes prohibitively small as the bead is moved just a few centimeters away from the Geiger

counter. This would restrict the size of our experimental workspace to a scale that is too small for implementing sensor networks and sensor mobility.

Instead of using actual radiation sources and Geiger counters, an emulation of the radiation detection process can be used for mesoscale experimentation with mobile ground robots in the lab setting. Specifically, we need a way to controllably emulate the physics of radiation emission in a way such that the observations of a nearby sensor mimic the response of a Geiger counter in the presence of radiation. Using an emulation should also allow for precise control of various physical parameter on both the emission and detection end such as source intensity, sensor/source separation, sensor size, etc.

One example of an experimental emulation that has been demonstrated in [19] uses a red light bulb in a field with mobile robots equipped with IR sensors. The light intensity measured by each robot is passed through a Poisson distribution filter as the mean for that sample. The filter returns a random number generated from a Poisson distribution with a mean of the measured light intensity. This works well because the IR sensors naturally pick up the ambient background light and the source light intensity also falls off like  $1/r^2$ . However, this is not much different from a simulation, which is doomed to succeed, so to speak. A critical component of experimentation is that it is an imperfect system and captures the potential “flaws” in the real world. In other words, experiments should be isolated from the assumptions made in the model. Our aim is to develop an emulation that inherently captures the physics of discrete emissions without the use of a filter.

The remainder of this thesis will discuss in detail exactly how this is achieved. Chapter 2 outlines the problem scope more thoroughly and breaks down the problem into various design constraints that need to be addressed. Chapter 3 describes exactly how the emulation works, how it meets the design specifications, and its various capabilities and limitations. Chapter 4 outlines the experimental results that verify the system performance, and the thesis concludes with Chapter 5.

## Chapter 2

### PROBLEM STATEMENT

Motivated by a need to augment the experimental efforts in networked radiation detection, the chief problem to be addressed in this thesis is how to enable those without the facilities to handle radioactive materials to conduct experiments. To avoid using fissile materials, an emulating proxy is needed to mimic the process of radiation emission and detection. The proxy used in place of fissile materials must be controllable so that it can be applied to various detection scenarios.

In order to better define the problem at hand, we must take a closer look at the Poisson process, which is at the heart of all weak signal detection. By definition, a Poisson process is a continuous-time counting process, where  $\{N(t), t \geq 0\}$  denotes the number of events (in our case gamma rays) that are observed since  $t = 0$ . It is further defined by the following properties:

- $N(0) = 0$ .
- Independent intervals: the number of events in disjoint intervals is mutually independent. That is if  $t_1 < t_2 < t_3 < t_4$ , then  $N(t_2 - t_1)$  and  $N(t_4 - t_3)$  are independent for a given Poisson process.
- Stationary increments: the probability distribution of events in any sub-interval ( $t^*$ ) is only dependent of the length of the interval  $N \equiv N(|t^*|)$ .
- No counted events occur simultaneously.
- The probability distribution of  $N(t)$  is a Poisson distribution:

$$\mathbf{P}(N(t) = k) = \frac{m(t)^k}{k!} e^{-m(t)}, \quad m(t) = \int_0^t \lambda(u) du, \quad k = 0, 1, 2, \dots$$

- The probability of time between events is exponentially distributed given by (1.1).
- The two Poisson processes we deal with in detection theory are defined as

$$\beta \equiv \beta(\vec{X}), \quad \vec{X} \in \mathbb{R}^3, \quad \text{and}$$

$$R_i(r, t) \triangleq f(r_i)\lambda_i(t), \quad f(r_i) \triangleq \frac{1}{1 + \left(\frac{r_i}{K_{1/2}}\right)^2} \quad (2.1)$$

Here, the background intensity  $\beta$  is only a function of spatial position, and is known to the sensor. This is often referred to as a background radiation map. Variable  $R_i$  is the intensity of the signal from source  $i$  and is separable into functions of position and time.<sup>1</sup> Variable  $r_i$  is the distance between the sensor and source  $i$ , and  $K_{1/2}$  is the distance at which its intensity falls off to half its maximum value ( $\lambda_i$ ). This form of function  $f(r_i)$ , suggested in [20], incorporates the  $1/r^2$  falloff but does not blow up at  $r_i \rightarrow 0$ . A key assumption that is being made about the source is that it emits gamma rays uniformly, meaning that  $R_i$  is not dependent on the direction of a sensor w.r.t. source  $i$ . Most concentrated “point sources” of radiation do emit uniformly, but it is possible that they can be housed in an enclosure with non-uniform shielding (e.g. a lead plate on one side). This is not usually predictable from an outside perspective, so we are forced to assume uniformity in most cases.

In our emulation we would like to have control over the following variables:

- $\beta(\vec{X})$ : Intensity and distribution of background Poisson process;
- $\lambda_i(\phi, t)$ : Total source emission as a function of direction (for shielding cases) and time;
- $K_{1/2}$ : Half-intensity distance is controlled by the area of the sensor;
- $r_i$ : Radial distance between the source and sensor.

---

<sup>1</sup> We will often take  $\lambda_i(t)$  to be constant, but this is the more general non-homogeneous representation.

The more control we have over these variables, the more versatile the emulation will be. If the sensor/source distance ( $r_i$ ) is fixed, for example, then the emulation would only be useful for static detection problems. The ability to use the emulation on mobile robots is critical for testing theory that is currently being developed.

## Chapter 3

### TECHNICAL APPROACH

#### 3.1 Device Design

The proposed solution consists of a laser pointer that produces short pulses of light to mimic the emission of discrete gamma rays. These pulses are modulated by a software program that draws random samples from a Poisson distribution with a desired mean. The downward facing laser beam is then reflected at a  $90^\circ$  angle by a mirror. The mirror is fixed to the shaft of a stepper motor which rotates to a random orientation for each laser pulse, thereby creating a  $360^\circ$  planar emission spectrum. Consequently, any light sensor (or array of sensors) that is positioned in the plane of emission only picks up a fraction of the laser pulses. And because the light sensor has a finite area of sensitivity, the fraction of laser pulses it receives (i.e. the source signal intensity) is dependent on its distance from the laser source. Figure 3.1 depicts a SolidWorks<sup>TM</sup> rendering of the device.

The system is controlled by a MATLAB<sup>TM</sup> function, and the pseudo-code can be found in Appendix A. The inputs are mean pulse frequency ( $\lambda$ , given in pulses/sec) and the length of the experiment (*RunTime*, given in seconds). After the laser, motor, and sensors have been initialized, a vector is generated, the elements of which are random numbers sampled from an exponential distribution with mean  $(1/\lambda)$ . The elements of this vector serve as the time that is waited between two consecutive laser pulses, as per the definition of the Poisson process defined in Chapter 2. After each laser pulse is emitted, the stepper motor rotates to a random angle and the software pauses for the time indicated by the next element of the wait-time vector. This is repeated until the experiment duration is reached.

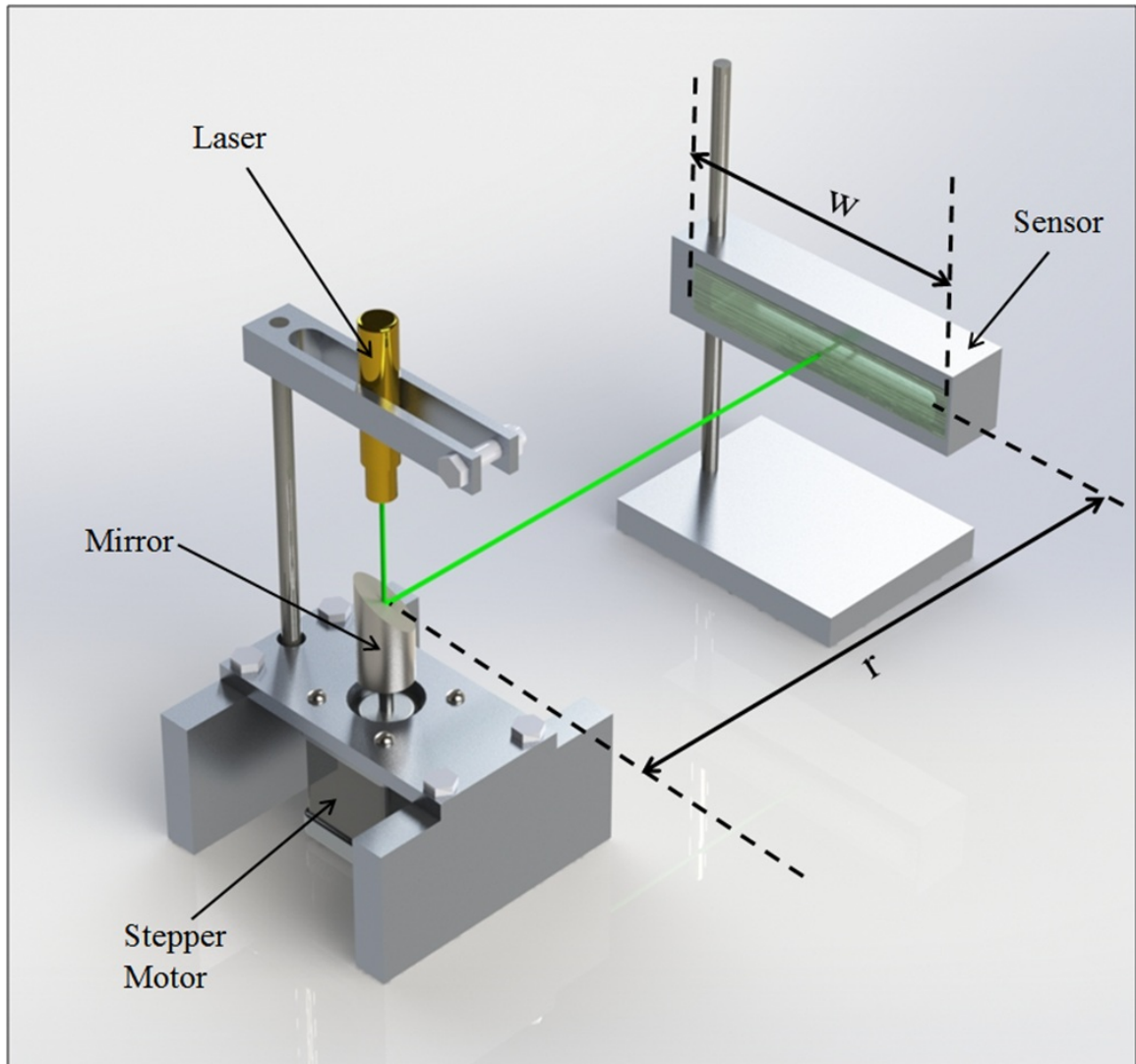


**Figure 3.1:** Solidworks<sup>TM</sup> rendering of the experimental setup:  $r$  is the distance between sensor and mirror;  $w$  is the sensitive width of sensor.

A light sensor positioned near the laser indicates a high light intensity when the laser beam is incident on it, and ambient levels at all other times. In order for it to behave like a Geiger counter, it must register the time stamp of each incident pulse. However, the light sensor works in a fundamentally different way than a Geiger counter because it is not a passive monitor. It can only return the light intensity value when interrogated by the software. This creates a problem because the sensor can only sample finite instants in time, which is not acceptable for measuring a continuous-time Poisson process. In other words, there is a chance that the sensor could *miss* a pulse if it occurs between queries. We can eliminate this problem by controlling the laser and sensor through the same software process, such that the sensor only checks for a light pulse if the laser is told to pulse. In this way, we can ensure that the sensor is “on” when the laser sends a pulse.

### 3.2 Directional Randomness

The randomness in direction we observe in radiation emission is caused by the decay of a high energy nucleus, resulting in a continuous range of emission in  $\mathbb{R}^3$ . We can come close to generating a continuous spectrum in  $\mathbb{R}^2$  with a stepper motor. The motor we are currently using has a resolution of 6400 steps/revolution, which is sufficiently fine to create this continuous effect. In other words, even at the farthest distance a sensor can be from the laser in our lab, there are still several consecutive angular steps that span across the width of the sensor.

At first, we tried to control the laser pulsing and mirror movement independently by having the mirror constantly in random motion. However, because the laser pulse has a finite duration (not like an instantaneous gamma ray), each pulse produced a diffracted beam when reflected by the moving mirror. This is not acceptable because the distance/intensity falloff relationship only holds for pulses restricted to 1D (i.e. each laser pulse must produce a dot, not a line). To overcome this problem, the stepper motor is synchronized with the laser pulses so that it only rotates to a random

location immediately after each pulse. This guarantees that the laser only pulses while the mirror is stationary but still maintains the randomness in direction.

This approach also allows for the possibility of imposing directional bias or non-uniformity in the emission such that  $\lambda = \lambda(\phi, t)$ . Recall the discussion on shielding and non-uniformity in Chapter 2. This capability is useful for experiments in which we want to observe the effect of shielding. To achieve this, instead of having the mirror rotate to a random location, it would be biased with a higher probability of rotating to certain angular regions. Another convenient use of this ability is for experiments when sensors are known to be restricted to a certain region. Discussed further in Section 3.6, the laser turns out to have a limit on the pulse frequency; so restricting pulses to the half plane ( $0^\circ < \phi < 180^\circ$ ), for example, allows us to effectively double the maximum source strength observed in that region.

### 3.3 Mixing Background and Source Signals

The laser device created has only one emitting source, but experiments require a background signal as well. There are a few ways in which we can generate (or effectively generate) two parallel Poisson processes ( $\beta$  and  $\lambda$ ). For the most restricted case of a fixed sensor and source (i.e.  $\frac{dr}{dt} = 0$ ), both  $\beta$  and  $\lambda$  can be generated directly with the laser by superposing their intensities such that the total intensity is the sum of source and background signals.

For the more general case in which the source and sensors can move,  $\beta$  cannot be generated with the laser because it too would dissipate over distance, which would not be in agreement with an assumption of a uniform ambient background. The most direct way to create the background emission is to simulate the background signal and send it directly to the sensor software. This can be done without using the light sensor as long as the detector cannot tell if a pulse is coming from  $\beta$  or from  $\lambda$ . Furthermore, if source localization can be attained, the radiation map  $\beta(\vec{X})$  can also be incorporated.

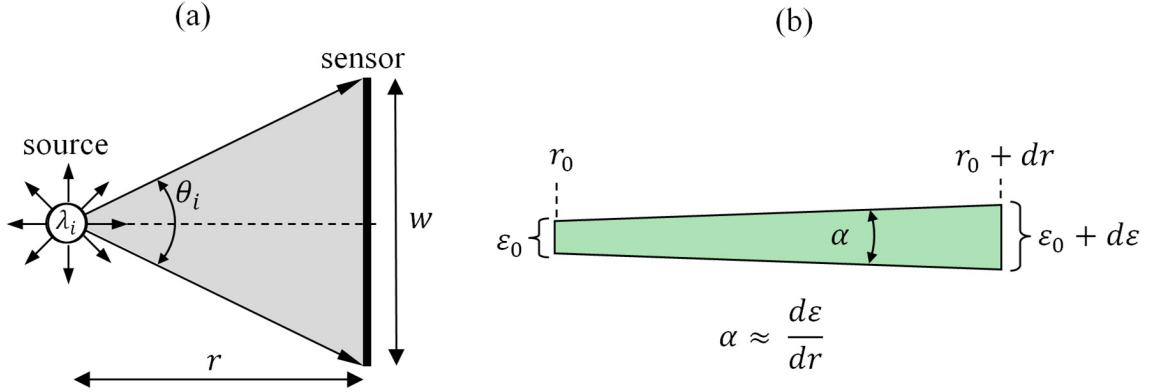


**Figure 3.2:** (a) Schematic of laser emission in  $\mathbb{R}^2$ ; (b) element of laser beam scattering

### 3.4 Distance from Sensor to Source

Recall from Section 1.2.3 that the intensity of radiation incident on a sensor exhibits a  $1/r^2$  falloff given by (2.1). For simplicity, our emulation is restricted to emission in  $\mathbb{R}^2$ , so the falloff will instead be proportional to  $1/r$ . This fundamental difference arises because in  $\mathbb{R}^3$  the sensor area creates a solid angle as viewed by the source (measured in radians squared); whereas a sensor in  $\mathbb{R}^2$  creates a standard angle to the source. Since the solid angle is given by  $\Omega \approx \alpha^2$  and  $\alpha \propto \frac{1}{r}$  ( $\alpha \ll 1$ ), it follows that the fractional incidence in  $\mathbb{R}^3$  is proportional to  $1/r^2$  but only proportional to  $1/r$  in  $\mathbb{R}^2$ . This is sufficient for experimentation, and we can easily extrapolate the effects observed in  $\mathbb{R}^2$  into the  $\mathbb{R}^3$  domain.

Let us examine more closely how well the  $1/r$  relation holds. Figure 3.2a shows a simplified schematic of the laser and sensor with a view orthogonal to the emission plane. Let's define the *fractional incidence* ( $f_{ik}(r)$ ) to be the angular scope ( $\theta_i$ ) of sensor  $k$  w.r.t. source  $i$  divided by the total angular range of emission (typically  $360^\circ$ ). At close range, the fractional incidence function  $f(r)$  is given by,

$$f(r) = \frac{1}{\pi} \tan^{-1} \left( \frac{w}{2r} \right). \quad (3.1)$$

However, as  $\frac{w}{r} \rightarrow 0$ , we have that

$$\lim_{\frac{w}{r} \rightarrow 0} f(r) = \frac{w}{2\pi r}. \quad (3.2)$$

Practically, this approximation is accurate to within 1% when  $w < 3r$ . This relationship also relies on two assumptions concerning the laser beam (refer to Fig. 3.2b):

- (i) that the width of the laser beam is significantly smaller than the sensor width, (i.e.,  $\varepsilon \ll w$ ), and
- (ii) that the scattering angle of the beam is significantly less than the incidence angle, (i.e.,  $\alpha \ll \theta_i$ ).

In our case, both assumptions are valid:

- (i)  $\varepsilon_{max} \approx 5$  mm,  $w_{min} \approx 50$  mm
- (ii)  $\alpha \approx 10^{-3}$  rad,  $\theta_{i\ min} \approx 0.02$  rad (at  $r = 10$  ft).

In summary, the sensor incidence will be proportional to  $1/r$  if  $3 < \frac{r}{w} < 100$  and  $w > 2$  inches. These requirements may be relaxed if a more focused laser is used.

### 3.5 Scaling

When running experiments with this laser device, we need to ensure that appropriate parameter scaling is used so that the light sensor collects the same amount of information as a Geiger counter would. Because the laser pulse frequency is limited by the rotation speed of the mirror and the laser pulse duration, our light detectors require larger scopes than typical radiation sensors. To establish a link between our experiments and an actual radiation detection scenario, these larger detectors can be viewed as an equivalent replacement of multiple smaller sensors. Consider  $n$  sensors of the same (this assumption can be relaxed) characteristic surface constant  $\chi$ , at distances  $r_1, \dots, r_n$  from a point source of intensity  $\alpha$ . On the plane, the perceived activity at the sensor will be

$$R_i = \frac{\chi\alpha}{1 + r_i} \quad .$$

(it will be  $r_i^2$  in 3D)

The whole distributed collection of sensors can be replaced by a single “equivalent” sensor at a distance  $r_0$  having a characteristic surface constant  $\chi_0$ . The latter is found by computing the “equivalent” component of each sensor when it is moved from distance  $r_i$  to distance  $r_0$ :

$$\frac{\chi\alpha}{1 + r_i} = \frac{\chi_i\alpha}{1 + r_0}, \quad \chi_i = \frac{\chi(1 + r_0)}{1 + r_i} \quad .$$

Thus, having all the sensors distributed at different distances should have the same collective effect as a single bigger sensor at  $r_0$ , with characteristic surface constant

$$\chi_0 = \sum_{i=1}^n \frac{\chi(1 + r_0)}{1 + r_i} \quad ,$$

yielding a perceived activity at the sensor’s end

$$R_0 = \frac{\alpha \sum_{i=1}^n \frac{\chi(1+r_0)}{1+r_i}}{1 + r_0} \quad .$$

The background signal can be scaled in the same way because it is proportional to the size of the sensor. For a uniform background, the “equivalent” background signal for the larger sensor is

$$\beta_0 = \beta \frac{\chi_0}{\chi} = \beta \sum_{i=1}^n \frac{1 + r_0}{1 + r_i} \quad .$$

Using these scaling transformations, we can use a larger sensor with the laser device in place of several smaller radiation sensors in our model of interest. Also, when dealing with mobile sources, we must scale the speed of the source and the observation window to produce equivalent information. For example, a source of activity  $\alpha$  traveling at a speed  $v$  past a stationary sensor is functionally equivalent to a source of activity

$2\alpha$  traveling at a speed  $2v$ . The information collected is the same, but one experiment takes twice as long. Due to the frequency limitations of the laser, we often need to extend the timescale of the experiment and reduce the traveling speed of the laser.

### 3.6 Computational Delays and Frequency Limitations

Recall from Section 3.1 that the laser pulsing sequence is generated by a vector of random numbers sampled from an exponential PDF. However, the pulsing statistics cannot be an exact Poisson process because there is a small time delay for each pulse. This delay ( $\delta t$ ) is the sum of the time it takes to rotate the mirror, turn the laser on and off, and compute one loop iteration in the software. The delay adds to the desired wait time, effectively shifting the Poisson distribution to the right. For our current hardware,  $\delta t$  is typically between 0.1 and 0.2 seconds, meaning that no two pulses can be separated by less than that amount of time. In theory, we could still generate a maximum frequency of  $1/\delta t$ , but it would not be exponentially distributed. Therefore, to maintain the distribution shape, it is better to use lower frequencies. For a given system of hardware, there is not much we can do to reduce  $\delta t$ , but we can scale back the experiment such that  $\lambda_s = k\lambda$ ,  $k < 1$ , and the time restrictions imposed on the decision center are also adjusted by the same factor.

The maximum frequency that should be used with the current hardware is 2 Hz or 120 cpm. The biggest contribution to the lag is the time it takes the laser to reach full intensity after being turned on. Lasers do not turn on instantly like most incandescent light bulbs—they take time to warm up. Higher frequencies can be achieved if a laser with lower latency is used.

## Chapter 4

### EXPERIMENTAL RESULTS

#### 4.1 Conforming to Poisson Statistics

As discussed in Chapter 3, there are two essential criteria that must be captured by this emulation for it to be an adequate radiation detection proxy: (1) it must produce a Poisson process at the sensor and (2) the intensity of the source signal (laser pulses) must dissipate over distance. The later is expected to fall off with the inverse of the distance because the laser pulses are restricted to  $\mathbb{R}^2$ .

It is typically assumed that radiation emissions conform to Poisson statistics, but for validating the performance of the laser device, we went straight to the source to compare it with an actual Geiger counter signal. The weakly radioactive source used is a bead of Vaseline glass (Fig. 4.1a), which contains small amounts of uranium oxide [21]. The bead has a diameter of about 1 cm and has an activity of less than 70 Bq/g, making it safe to handle. The Geiger counter used is a GM-10 from Black Cat Systems<sup>TM</sup> (Fig. 4.1b), which has a 1 cm<sup>2</sup> scope [22]. It measures a background radiation level of about 10-15 cpm in the lab, and over 50 cpm when touching the Vaseline bead.

To test the signal statistics, the distribution of background radiation collected by the Geiger counter was compared with the laser device. The Geiger counter was left to collect background measurements for a 24-hour period, during which it recorded over 18,000 counts with a mean frequency of 12.7 cpm. The output signal from the Geiger counter is a chronological time stamp vector of gamma ray events, which can then be manipulated to produce a vector of times between consecutive events. This theoretically should be exponentially distributed. The data was sorted into 1 second

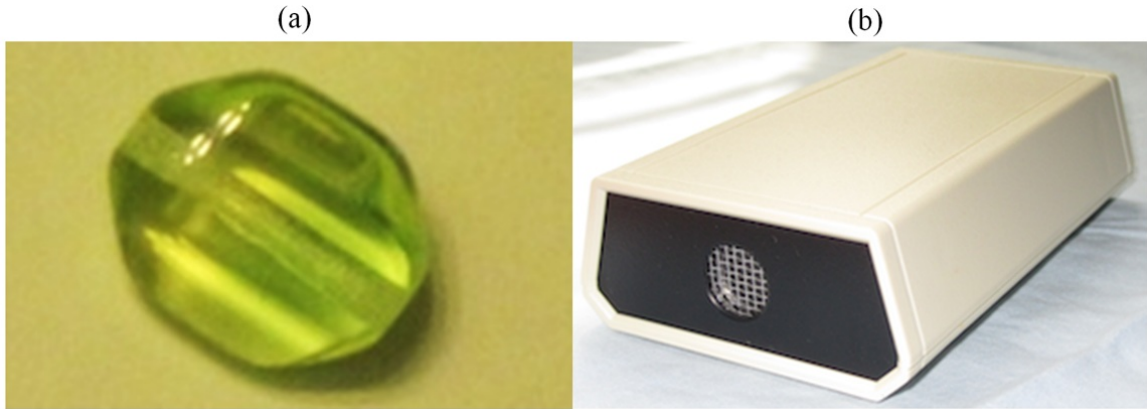


**Figure 4.1:** (a) bead of Vaseline glass; (b) Geiger counter

bins and are plotted against relative frequency. Figure 4.2 shows the result of an exponential regression to the data which is a very strong fit ( $R^2 = 0.9993$ ), as expected.

In a similar manner, the laser device was set up to run a long background trial, with the light sensor at an average distance from the mirror.<sup>1</sup> Over a three-hour period, the sensor collected over 6000 counts with a mean frequency of 36 cpm. The exponential fit to this data is shown in Fig. 4.3, which also displays strong convergence ( $R^2 = 0.997$ ). Note: recall from Section 3.6 that each laser pulse takes a finite amount of time, which essentially shifts the desired exponential PDF by  $(\delta t)$  to the right. One way to compensate for this lag is to simply subtract the measured error  $(\delta t)$  from each wait-time datum measured by the sensor, shifting the PDF back to the left.<sup>2</sup> The data in Fig. 4.3 has been adjusted using this technique.

The comparison of Figs. 4.2 and 4.3 indicates that the device is capable of producing the Poisson process. An interesting observation made during this experiment was the fluctuations of the background radiation over time. Even though the Geiger

---

<sup>1</sup> The background signal will not typically be generated by the laser; it will usually be simulated and with the source signal directly in the software. This will be exponentially distributed by design, so this test instead reflects the accuracy of the source signal.

<sup>2</sup> This technique cannot be used in all applications, so it is best to be cautious and use lower pulse frequencies whenever possible.

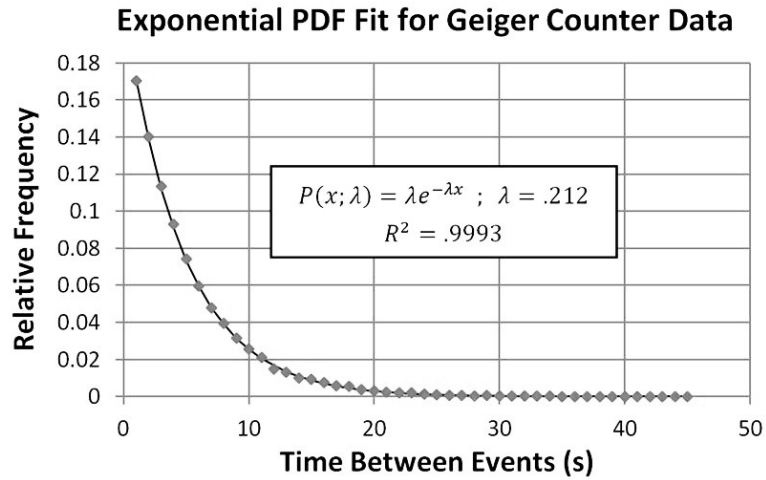


**Figure 4.2:** A 24-hour sample of background radiation ( $n \approx 18,000$ ) as measured by a Geiger counter

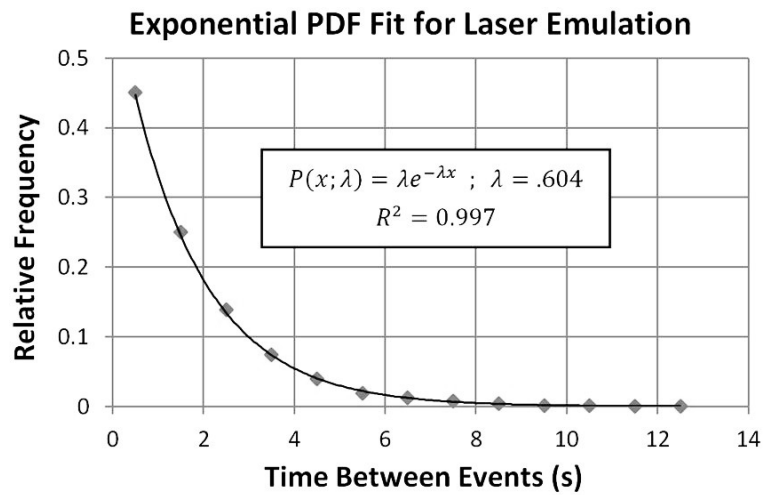


**Figure 4.3:** A three-hour sample from the laser device emitting Poisson background ( $n \approx 6,000$ )

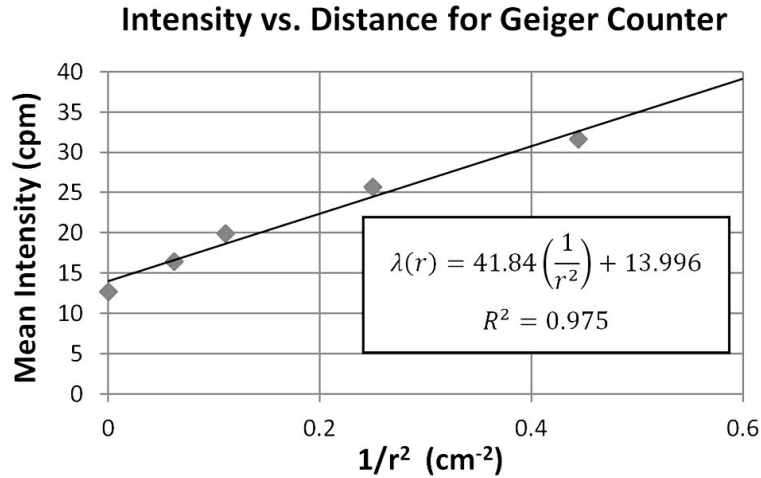


**Figure 4.4:** Geiger counter samples in range of radioactive glass bead

counter was left in the same position for the full 24 hours, the background intensity seemed to fluctuate significantly throughout the day, with higher intensities during the day and lower intensities at night (ranging 10 - 15 cpm). This highlights the stability advantage of our controlled emulation.

Now we can explore the validity of our second requirement: the distance relationship. The Vaseline bead was placed in front of the Geiger counter and the signal was measured for 20 minutes at each of 5 different distances. Figure 4.4 shows a plot of mean intensity (in cpm) vs.  $1/r^2$  for the 5 samples collected, which exhibits a strong linear regression correlation ( $R^2 = 0.975$ ). The data does show a slight downward curvature, which could be caused by a combination of two effects: (1) the closest distances of 1.5 and 2 cm probably violate the point source assumption and (2) the actual Geiger tube is inset into the Geiger counter housing meaning that  $r$  should be measured to a point behind the face of the Geiger counter. Also, the fit would likely be better if longer samples were taken. The intercept of the linear regression represents the background level (i.e. as  $r \rightarrow \infty$ ), which is close to the background measurements in Fig. 4.2.

For the laser device, the same experimental procedure was run for 9 different

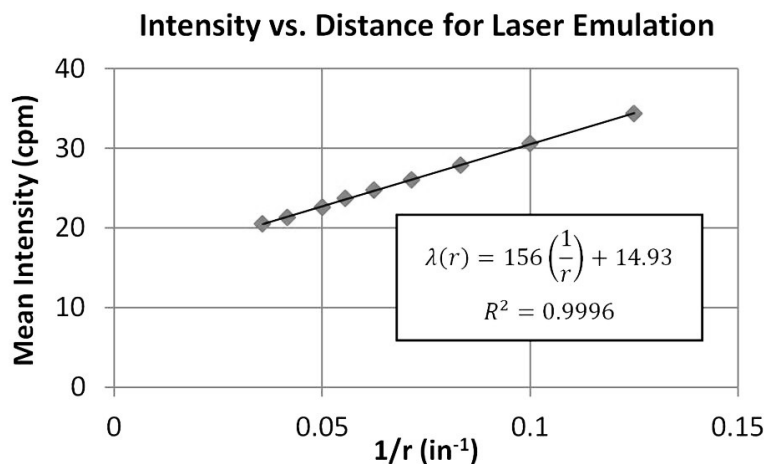


**Figure 4.5:** Mean intensity at sensor  $(\lambda + \beta)$  vs. source distance

distances between 8 inches and 28 inches. A background signal with intensity 15 cpm was simulated and added to the laser pulses picked up from the source. Each trial was run for three hours and the mean intensities are plotted in Fig 4.5. The linear regression shows a very strong relationship between mean intensity and  $1/r$ , and the y-intercept reflects the preset background intensity. Recall from section 3.4 that the distance falloff for this device is proportional to  $1/r$  because the emissions are confined to  $\mathbb{R}^2$ .

## 4.2 Application to Static Detection

Now that the necessary criteria for emulation have been addressed in isolation, the device can be applied to the problem of interest: detection. As a preliminary example, the device was applied to a fixed interval detection scenario, and its performance was compared to a similar experiment using the Vaseline bead.

The fixed interval detection problem typically arises when the source trajectory is known, such that a sensor can isolate a window of time in which it is exposed to the source. For example, a source that travels past a stationary sensor does not register any counts well before it arrives or well after it has left, so the sensor will provide the most meaningful measurements in some window of time  $(t_0 < t < T)$  bounded

by the proximity of the source. Instead of a dynamic likelihood ratio that evolves as information is collected, for fixed intervals we just need to compute the likelihood ratio once all of the data has been collected and compare it to a preset threshold. If the likelihood ratio is above the threshold, we declare a detection. The likelihood ratio ( $L_T$ ) we use here is calculated with the following formulas (see [20]):

$$\begin{aligned}\nu_i(t) &= \frac{\chi\alpha}{r_i(t)^2} \\ \mu_i(t) &= 1 + \frac{\nu_i(t)}{\beta} \\ L_T &= \exp\left(-\sum_{i=1}^k \int_0^T \nu_i(s) ds\right) \prod_{i=1}^k \prod_{ni=1}^{N_{Ti}} \mu_i(t_{ni})\end{aligned}$$

where  $\chi$ ,  $\alpha$ ,  $\beta$ ,  $r_i(t)$ ,  $T$ ,  $N_{Ti}$ , and  $t_{ni}$  are defined as:

- $\chi$  : shape factor of the sensor (characteristic surface constant)
- $\alpha$  : mean emission frequency of the source
- $\beta$  : mean background frequency observed by the sensor
- $r_i(t)$  : distance between the source and sensor  $i$
- $T$  : time span of collected data
- $N_{Ti}$  : total number of gamma rays received by sensor  $i$  during  $T$
- $t_{ni}$  : time point when sensor  $i$  receives the  $ni_{th}$  gamma ray

This calculation can be used for cases with one mobile source and  $k$  mobile sensors. However, in our experiment with the weak source and Geiger counter, we use only one sensor, where both sensor and source are static. So the likelihood ratio

formulas are simplified to:

$$\begin{aligned}\nu &= \frac{\chi\alpha}{r^2} \\ \mu &= 1 + \frac{\nu}{\beta} \\ L_T &= \exp(-\nu T)\mu^{N_T} .\end{aligned}$$

Recall our discussion in section 1.2.4 about the two types of errors associated with binary detection: false positives and false negatives. The metric we use for comparison between the Geiger counter and laser device is the *rate* or *probability* of false negatives, or missed detections. By computing the likelihood ratio for a large number of observations, we can formulate a relationship between detection probability and threshold. This process is repeated for various distances to develop a family of curves that describe how detection probability falls off for higher thresholds. To validate the laser device as an effective proxy, it must produce similar curves as the Vaseline bead and Geiger counter.

For this static detection experiment, the Vaseline bead and Geiger counter are separated from 1 cm to 3 cm apart. At each distance, 100 samples are collected that are each one minute long (i.e.  $T = 1$  min). The total number of gamma rays collected by the Geiger counter ( $N_T$ ) is recorded for each sample. In this case, the sensor shape factor ( $\chi$ ), the source intensity ( $\alpha$ ), and the background level ( $\beta$ ) are all assumed to be known, so  $\nu$  and  $\mu$  can be calculated for each sample as well as their respective likelihood ratio ( $L_T$ ). Finally, the probability of detection at each distance is estimated as the percentage of samples that yield likelihood ratios higher than a given threshold.

Figure 4.6 shows the resulting family of detection curves for the bead and Geiger counter at distances 1, 1.5, 2, 2.5, and 3 cm. The curves are downward sloping, confirming the inverse relationship between detection probability and threshold that we expected. Not surprisingly, the probability of detection also drops off more abruptly at farther distances, which means that smaller thresholds must be used to detect more distant sources with the same probability. However, using smaller thresholds incurs a

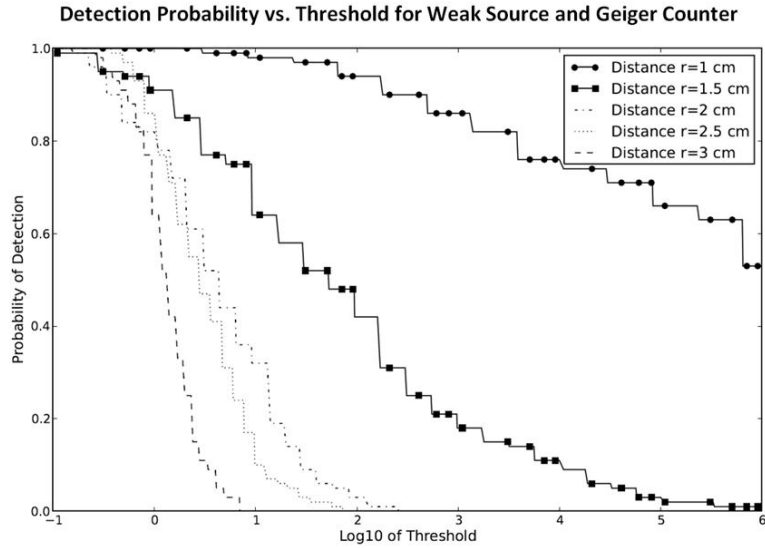


**Figure 4.6:** Probability of detection vs. likelihood ratio threshold (log10 scale) in bead experiment at distances 1, 1.5, 2, 2.5, and 3 cm

higher rate of false positives. So again, getting the sensors close to the source is critical for minimizing the detection errors.

For the sake of comparison, we would like to produce the same type of curves in Fig. 4.6 with the laser device. However, because the laser device lives in  $\mathbb{R}^2$ , the adjusted  $\nu$  value is computed as,

$$\nu = \frac{\chi\alpha}{r} = \frac{\lambda w}{2\pi r} \quad .$$

So to generate the same curves with the laser device, we must match the  $\nu$  values. Since we used a linear sequence of distances for the bead/Geiger counter experiment, it follows that we must use a quadratic sequence of distances for the laser system (e.g. 4, 9, 16, 25, and 36 inches). At these distances, each sample is collected for one minute with a pulse frequency of 2.78 Hz and a sensor scope of 4 inches. The signal measured by the light sensor is added to a background signal to produce similar  $\mu$  and  $N_T$  values. The results shown in Fig. 4.7 closely resemble the curves in Fig. 4.6. Therefore, the device is capable of producing the data we need for detection experiments.

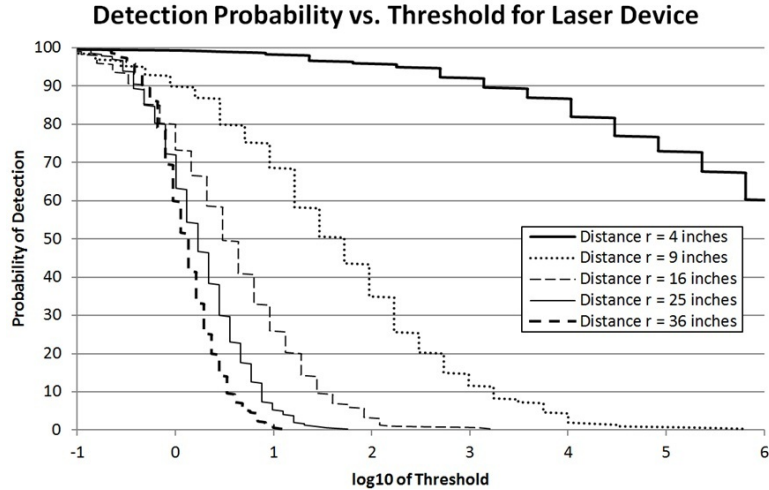


**Figure 4.7:** Probability of detection vs. likelihood ratio threshold ( $\log_{10}$  scale) from experiments with the laser device at distances 4, 9, 16, 25, and 36 inches

### 4.3 Detection of a Mobile Source

Finally, we are ready to apply the laser emulation to an experiment with mobility. The ultimate goal is to be able to use this device for any type of 2D experiment in which the laser and light sensors are mobile. To achieve mobility, the laser device and light sensors were integrated onto two different mobile robots (see Fig. 4.8). The robot used for the laser is an iCreate<sup>TM</sup> (see Fig. 4.8a) from iRobot<sup>TM</sup> (same as the Roomba<sup>TM</sup> without the vacuum), which was modified to have multiple platforms. The top platform carries the laser device and circuitry hardware, the middle platform is where we place the laptop that controls the laser device, and the batteries for the stepper motor and laser are housed in the lower cargo bay. The iCreate<sup>TM</sup> was chosen to carry the laser because it can fit an on-board laptop, it is user friendly, it can move very slowly (down to about 0.03 m/s), and it has built-in encoders that are automatically used to guide the robot along a prescribed trajectory. The robot that was used to carry the mobile sensor was a Corobot<sup>TM</sup> (see Fig. 4.8b), which was modified to have smaller wheels. The smaller and more rigid wheels have lower friction than the soft tires, which allows the Corobot<sup>TM</sup> to move slower to follow the source.

The experiment conducted with the mobile robots was a simple scenario with



**Figure 4.8:** (a) laser device mounted on the iCreate<sup>TM</sup>; (b) light sensor mounted on the Corobot<sup>TM</sup>

a constant velocity source moving in a straight line. Figure 4.9 shows a schematic of this setup. A combination of stationary and mobile sensors were arranged along a straight line parallel to the trajectory of the source. One sensor was made mobile while four sensors were stationary. The mobile sensor is told to track the laser source along a parallel trajectory. To avoid sensors “shadowing” each other, the mobile sensor moves on the opposite side of the laser in an equidistant parallel line. The laser source travels a total distance of 3 meters at 0.05 m/s, and the static sensors are located at  $x = 0.5, 1.5, 2.5,$  and 3 meters from the start of the source trajectory. Within each 60-second long trial, the data collected from each sensor is recorded as the total number of laser pulses received. This is added to a random background signal so the total reported signal at each sensor is the sum on laser pulses received and background counts simulated. A mean source frequency of 2Hz is generated by the laser and each sensor has a width of 16 inches. A picture of what this experiment looks like is shown in Fig. 4.10.

The data collected from this experiment was interpreted in a similar way as the fixed interval static detection example in the previous section. Based on the number of counts measured during each 60-second trial, the log-likelihood ratio was computed for

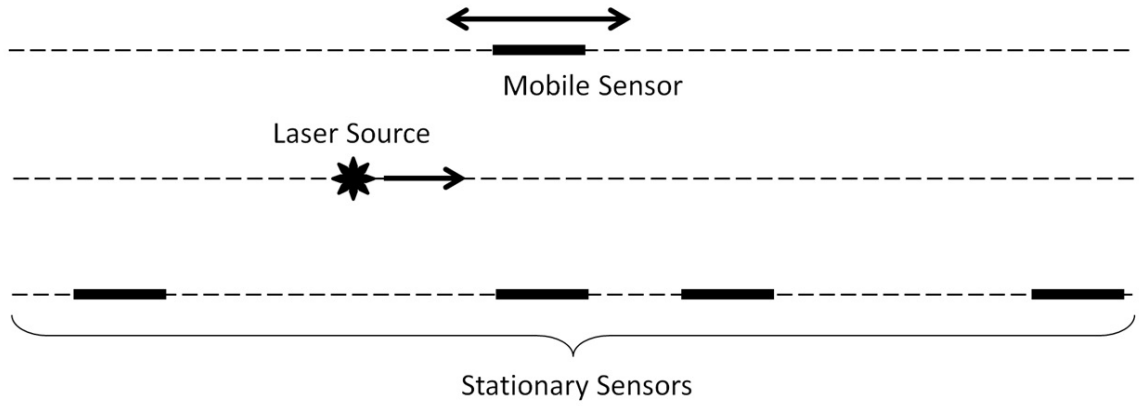


**Figure 4.9:** Schematic of experiment with 1D source movement

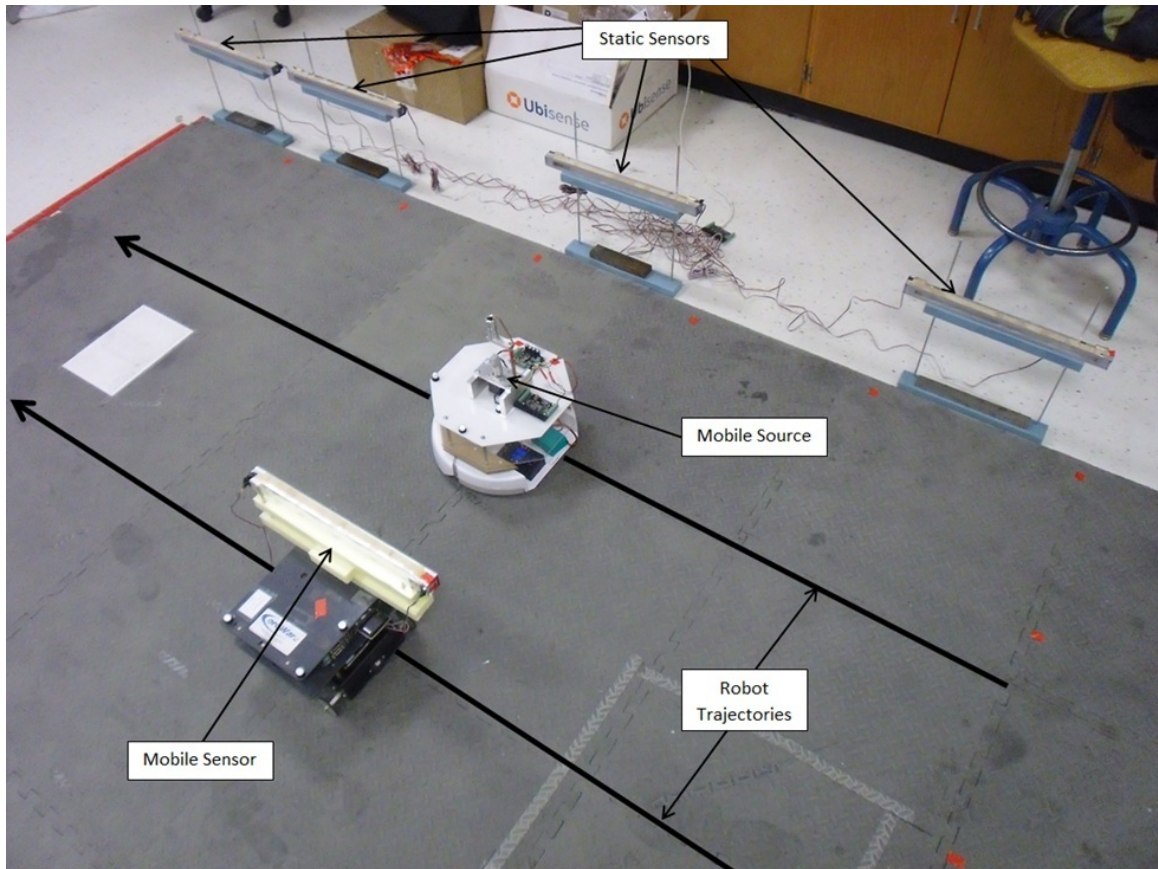


**Figure 4.10:** Picture of a mobile detection experiment with one mobile sensor and four stationary sensors

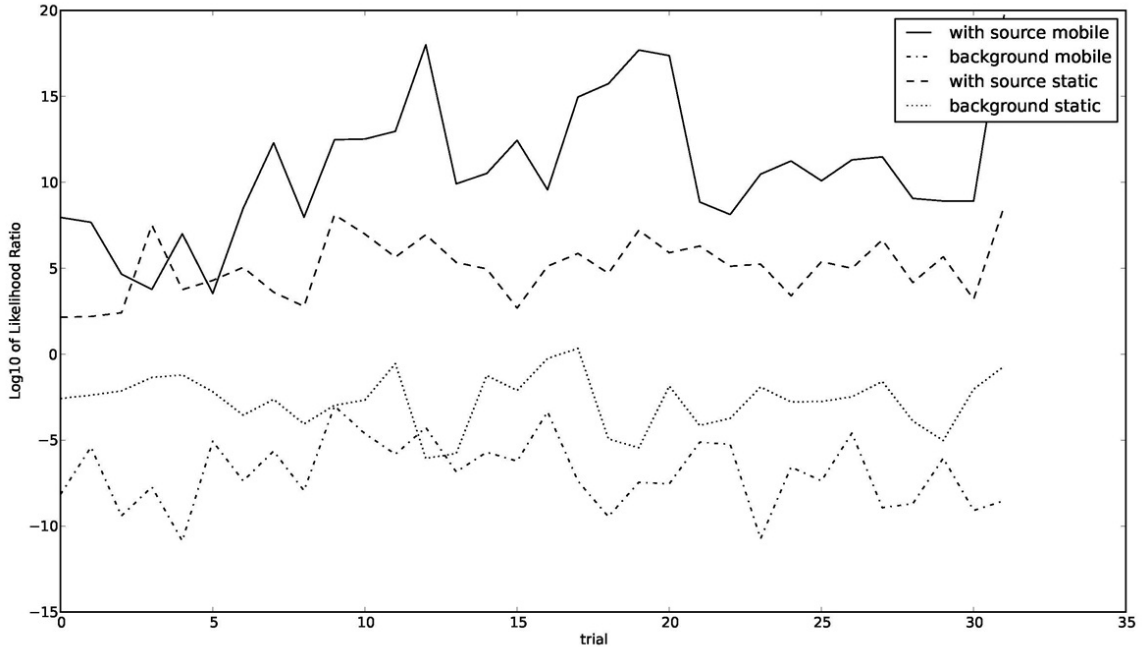


**Figure 4.11:** Log likelihood ratios based on data collected from 4 sensor groupings: two from just the four static sensors (one just background and one including the source), and two from all 5 sensors (one just background and one including the source)

each of the the 31 trials run. These results are shown in Fig. 4.11. The data gathered from each experiment were segmented into four categories to highlight the benefit of sensor mobility. The top line shows the the log-likelihood ratios for data collected from all five sensors including both background and source signals. The second line from the top reflects the source and background signals as measured by just the four static sensors. The two lower data series show the log-likelihood ratios computed for just the background signal with data from just the four static sensors, and all 5 sensors.

The first thing we notice about the lines in Fig. 4.11 is that the series including the data from the mobile sensor significantly increases the likelihood ratios. Without the mobile sensor, the likelihood ratios average around  $10^5$ , but with the data from the mobile sensor, the likelihood ratios are much higher averaging around  $10^{10}$ . This tells us that there is a much higher probability of detection when the mobile sensor is

added. Another interesting observation is that the likelihood ratios computed based on just the background signal are lower when the mobile sensor is included (from  $10^{-3}$  to  $10^{-7}$ ). This is not an effect of mobility because mobile sensors presumably measure the same background intensity as static sensors. Rather, it is an artifact of simply adding more sensors and thereby collecting more data. Nonetheless, the lower background likelihood ratios are desirable for reducing the rate of false positives.

In this example, sensor mobility does not exactly allow the mobile sensor to get closer to the source—it is still confined to the same line as the static sensors. The reason that it is so powerful is that it can move as close as possible to the source *for as long as possible*. The static sensors only collect data from this minimum distance configuration for an instant in time, and the measured source signal drops off significantly as the source moves away. By “tracking” the source, the mobile sensor collected about 3-5 times as many counts as each stationary sensor during the 60 second window.

Using a combination of static and mobile sensors also has advantages from a resource allocation perspective. Consider an application of monitoring a roadway with high traffic volume at a way-point by a network of sensors. If all of the sensors are static, they may not be able to pick up as much information about the environment or distinguish a specific vehicle as the source of elevated radiation levels. Using all mobile sensors is also inefficient because the environment may have too many vehicles to track them all. For such an application, a group of static sensors can be used to passively monitor the environment and alert idling mobile sensors to further inspect suspicious targets. This hierarchical technique is an efficient way to zone in on potential sources in a crowded environment, which would presumably lead to rerouting suspicious targets for a more detailed inspection.

## Chapter 5

### CONCLUSION

Based on the fundamental principals of the Poisson process used to model weak radiation detection, an emulation process has been developed as a proxy for experimentation with actual radioactive material. To improve the detection capabilities of weak signals by exploring cases of mobile sensor networks, this device will help those without the ability to handle fissile materials run experiments in a safe environment. A laser is modulated to create short pulses of light that follow Poisson statistics, and a rotating mirror reflects each pulse in a random planar direction. By collapsing the emissions from the  $\mathbb{R}^3$  domain to  $\mathbb{R}^2$ , we inherently change the way radiation density dissipates as the sensor is moved farther from the source. However, the Poisson process and directional randomness are captured with this device. Thus it can still be used to run the same detection experiments as a real radiation sensor / source as long as we tell the sensor to expect a distance falloff of  $1/r$  instead of  $1/r^2$ . Preliminary testing verified that the laser device can in fact recreate the Poisson process of interest. It also yielded agreeable results during a static detection experiments. Finally, we saw a simple example of how this device might be used in the future with mobile sensor networks.

In general, this device is capable of being used for experiments in 2D, not just restricted to motion along a line. Practically, reliable 2D motion can only be achieved with position feedback from the motion capture system. The next step could be to put reflective markers on the robots and set up a trajectory following program. When permitting 2D motion with the robots, it is also important to remember that the sensors do have a certain orientation and can only capture laser pulses that come through the front, not unlike radiation sensors. So if there is a chance that the source

could move behind the sensor, it may be helpful to incorporate some sort tracking mechanism to ensure that the sensor is always “facing” the source. Another way this could be approached is by developing omnidirectional sensors that can detect laser pulses coming from all directions equally. Finally, the attainable emission frequency can be increased by upgrading the hardware. The most influential upgrade could be using a more responsive type of laser, which can be turned on and off quicker. Aside from that, we could try using multiple lasers and mirrors to increase the total amount of pulses that can be generated. In most cases however, the robots can move slow enough to collect enough data.

## REFERENCES

- [1] R. Vartabedian. U.S. to install new nuclear detectors at ports, 2006.
- [2] A. Papoulis. *Probability, Random Variables, and Stochastic Processes*. McGraw Hill, 1965.
- [3] R.A. Cortez, X. Papageorgiou, H.G. Tanner, A.V. Klimentko, K.N. Borozdin, R. Lumia, and W.C. Priedhorsky. Smart radiation sensor management; radiation search and mapping using mobile robots. *IEEE Robotics & Automation Magazine*, 15(3):85–93, 2008.
- [4] Robert J. Nemzek, Jared S. Dreicer, David C. Torney, and Tony T. Warnock. Distributed sensor networks for detection of mobile radioactive sources. *IEEE Transactions on Nuclear Science*, 51(4):1693–1700, 2004.
- [5] R.C. Byrd, J.M. Moss, W.C. Priedhorsky, C.A. Pura, G. W. Richter, K.J. Saeger, W.R. Scarlett, S.C. Scott, and R.L. Wagner Jr. Nuclear detection to prevent or defeat clandestine nuclear attack. *IEEE Sensors Journal*, 5(4):593–609, 2005.
- [6] A. Wald. Sequential tests of statistical hypotheses. *Annals of Mathematical Statistics*, 16:117–186, 1945.
- [7] M. Kulldorff, R.L. Davis, M. Kolczak, E. Lewis, T. Lieu, and R. Pkatt. A maximized sequential probability ratio test for drug and vaccine safety surveillance. *Sequential Analysis*, 30:58–78, 2011.
- [8] I. Bar-David. Communication under the poisson regime. *IEEE Transactions on Information Theory*, 15:31–37, 1969.
- [9] R.M. Gagliardi and S. Karp. M-ary Poisson detection and optical communications. *IEEE Transactions on Communication Technology*, 17:208–216, 1969.
- [10] A.W. Lam and A.M. Hussain. Performance analysis of direct-detection optical cdma communication systems with avalanche photodiodes. *IEEE Transactions on Communications*, 40:810–820, 1992.
- [11] M.C. Teich and S. Rosenberg. Photocounting array receivers for optical communication through the lognormal atmospheric channel: optimum and suboptimum receiver structures. *Journal of Applied Optics*, 12:2616–2623, 1973.

- [12] S. Verdu. Multiple-access channels with point-process observations: optimum demodulation. *IEEE Transactions on Information Theory*, 32:642–651, 1986.
- [13] G. Peskir and A.N. Shiryaev. Sequential testing problems for Poisson process. *Annals of Statistics*, 28:837–859, 2000.
- [14] H. Vincent Poor. *An Introduction to Signal Detection and Estimation*. Springer-Verlag, second edition, 1994.
- [15] Sean M. Brennan, Angela M. Mielke, and David C. Torney. Radioactive source detection by sensor networks. *IEEE Transactions on Nuclear Science*, 52(3):813–819, 2005.
- [16] D.L. Stephens Jr. and A.J. Peurrung. Detection of moving radioactive sources using sensor networks. *IEEE Transactions on Nuclear Science*, 51(5):2273–2278, 2004.
- [17] Ashok Sundaresan, Pramod K. Varshney, and Nageswara S. V. Rao. Distributed detection of a nuclear radioactive source using fusion of correlated decisions. In *Proceedings of the International Conference on Information Fusion*, pages 1–7. IEEE, 2007.
- [18] A.V. Klimenko, W.C. Priedhorsky, H. Tanner, K.N. Borozdin, and N. Hengartner. *Intelligent Sensor Management in Nuclear Searches and Radiological Surveys*, pages 21–22. 2006.
- [19] R. A. Cortez, H. G. Tanner, R. Lumia, and C. T. Abdallah. Information surfing for radiation map building. *International Journal of Robotics and Automation*, 26(1):4–12, 2011.
- [20] Chetan D. Pahlajani, Ioannis Poulakakis, and Herbert G. Tanner. Decision making in a sensor network with poisson process observations. In *IEEE Conference on Decision and Control*, (submitted), 2012.
- [21] Black Cat Systems. Vaseline glass bead geiger counter radioactive test source, 2012.
- [22] Black Cat Systems. Gm-10 Geiger counter radiation detector, 2012.

## Appendix

### MATLAB™ CONTROL PSEUDOCODE

```
function = PoissonEmissions(lambda,RunTime)

establish connection with hardware

if connection has been established:

    set bounds for stepper motor velocity, acceleration,
    and current.
    engage stepper motor
    collect light sensor values and set ambient threshold value
    create "WaitTime" vector of random numbers sampled from the
    exponential distribution with mean 1/lambda

    i = 1;
    start timer

    while timer < RunTime
        pause for WaitTime(i)
        rotate mirror to random direction
        turn laser on
        pause for 0.15 seconds
        get sensor readings - record count if greater than threshold
        turn laser off
        i = i + 1
    end

else
    failed to establish hardware communication - terminate program
end

disengage stepper motor and stop communication with hardware

end
```